HiLL PUBLISHING

OAJRC Material Science, 2024, 6(1), 1-11
https://www.hillpublisher.com/journals/oajrcms/
ISSN Online: 2632-2072

Optical Constants of Nanofilms for Spectrally Selective Windows

Winston T. Ireeta[1], Edward Bwayo[1,2,*], Daniel Mukiibi[1], Denis Okello[1], Willy Okullo[1], Robert Lugolole[1]

[1]Department of Physics, School of Physical Sciences, College of Natural Sciences, Makerere University, Kampala, Uganda.
[2]Department of Physics, Faculty of Science, Muni University, Arua, Uganda.

How to cite this paper: Winston T. Ireeta, Edward Bwayo, Daniel Mukiibi, Denis Okello, Willy Okullo, Robert Lugolole. (2024) Optical Constants of Nanofilms for Spectrally Selective Windows. *OAJRC Material Science*, 6(1), 1-11.
DOI: 10.26855/oajrcms.2024.03.001

Received: February 8, 2024
Accepted: March 5, 2024
Published: April 2, 2024

***Corresponding author:** Edward Bwayo, Department of Physics, School of Physical Sciences, College of Natural Sciences, Makerere University, Kampala, Uganda; Department of Physics, Faculty of Science, Muni University, Arua, Uganda.

Abstract

In this work, a spectral analysis of the effect of deposition angle on the optical constants for optically selective windows was carried out. The coatings of ZnS/Ag nanostructures were deposited on glass substrates from 0º to 60º. The measured transmittance increased with an increase in the deposition angle of silver nanofilms in the visible region but decreased with an increase in the deposition of silver in the infrared region. The transmittance decreased with an increase in the deposition angle of zinc sulfide in the visible region. Still, it increased with an increase in the deposition angle of zinc sulfide in the infrared region. The reflectance decreased with an increase in the deposition angle of silver nanoparticles in the visible region but decreased with an increase in the deposition angle of zinc sulfide. The effective refractive index increased from 3.25 in the visible spectrum to 6.2 in the infrared spectrum. The low values of the effective refractive index at visible wavelengths imply that the nanofilms were transparent to visible light. The extinction coefficient increased from an average of 0.2 at a wavelength of 400nm toward the infrared spectral band. The increase in deposition of ZnS did not significantly affect the energy band gap. However, the increase in the deposition angle of silver increased the energy band of the nanofilms from 3.52 to 3.99 eV.

Keywords

Deposition angle, transmittance, reflectance, refractive index, extinction coefficient, energy band gap

1. Introduction

The performance of windows and other fenestrations on buildings [1] plays an important role in controlling the rate of heat accumulation inside a building. Although several devices such as electronic air conditioners have been made to regulate indoor temperature [2, 3], it is desirable to employ other less costly mechanisms to reduce the transmission of infrared thermal radiation into the building. Therefore, the spectral and optical properties of glass used on windows and doors should be tailored to block the thermally energetic infrared radiation but at the same time allow in enough visible light [3-7].

The microstructure of the thin films on the substrate during physical vapor deposition depends on the direction or inclination of incident vapor flux onto the substrate. At the normal incidence of the vapor flux, a relatively homogeneous structure is formed [8, 9]. At elevated angles of deposition, i.e., at oblique angles, the film homogeneity tends to be distorted. This is because, during oblique deposition, particles arrive on the substrate surface at different times [10]. The initially attached molecules tend to shield the preceding vapour molecules from direct adhesion onto the substrate surface.

This leads to the formation of inclined nano-columns oriented in the direction of vapour [11-13]. The nano-columns form a porous microstructure different from the film formed at normal incidence. The inclination of columns affects the material's density, spectral and optical properties, and electrical properties [14-17].

When an electromagnetic field interacts with a dielectric material [18], there is charge polarization whose degree of polarization depends on the strength of the field and the intrinsic complex electric susceptibility and refractive index. However, the refractive index of the material directly affects the optical path length, phase, and reflectance properties of an optical interface. The reflectance that occurs at an optical interface at normal incidence is defined by equation (1).

$$R = \left(\frac{n_p - n_m}{n_p + n_m}\right) \tag{1}$$

where R is the reflectance, n_p is the refractive indices of the substrate and n_m is the refractive index of the incident medium. The refractive index n is related to the extinction coefficient k by the expression:

$$\bar{n} = n - ik \tag{2}$$

$\bar{n}$ represents the complex refractive index of the material. The refractive index n can be calculated from the measured reflectance data by equation 3 as follows [19-20];

$$n = \frac{(1+\sqrt{R})}{(1-\sqrt{R})} \tag{3}$$

During the transmission of an electromagnetic wave through a material, there is absorption which results in loss in intensity. This absorption loss is quantified by the extinction coefficient of the material and is dependent on [20] the absorption coefficient α, and the wavelength λ , thus;

$$k = \frac{\alpha\lambda}{4\pi} \tag{4}$$

where the absorption coefficient in equation (4) is given by;

$$\alpha = 2.3026\frac{A}{d} \tag{5}$$

where A is the calculated absorbance, and d is the film thickness.

During the deposition of very thin metallic nanoparticles [20], such as silver (Ag), there is a tendency for the nanoparticles to permeate into the dielectric material to form hybrid optical constants. The silver nanoparticles therefore fuse with zinc sulphide (ZnS) to form the hybrid ZnS/Ag multilayer structures [21] with distinct optical properties.

When light energy is incident on matter, it is either reflected, transmitted, or absorbed. The quantum of light energy absorbed triggers the excitation of valence electrons. The energetic valence electrons will move from the valence band to the conduction band across an energy band gap. The size of the energy band gap helps in explaining the optical properties and chemical activity of the semiconductors. However, the energy band gap is determined according to equation (6) developed by Tauc's method [22, 23];

$$(\alpha h\upsilon) = B(h\upsilon - E_g)^n \tag{6}$$

The constants h, υ, E_g stand for the Planck's constant, the photon's frequency, and the band gap energy respectively. B is also constant determined from the slope of the Tauc plot along the linear portion of the graph. The factor n depends on the nature of the electronic transition and is equal to 1⁄2 or 2 for the direct and indirect transition band gaps, respectively. The absorption coefficient α was calculated from the transmittance T, and reflectance R values [24] of the ZnS/Ag as follows:

$$\alpha = \frac{1}{d} ln\left(\frac{(1-R)^2}{T}\right) \tag{7}$$

where d is the film thickness.

When light energy is absorbed by an electron at the top of the valence band, the electron energy increases and it is propelled to the conduction band [25]. During this transition across the energy gap, the density of electronic states in both the valence and conduction bands tails into the energy gap. This phenomenon occurs as a result of the disorder generated by the presence of localized tail states, which originate from the presence of defects in film microstructure [24, 26]. Additionally, when electrons in the conduction band are subjected to an external electromagnetic field, they absorb energy, and the surface electrons are set into electrical oscillations. These oscillations result in the formation of localized surface plasmons on the surface of the metal [27].

The excitation of surface plasmons results in charge polarization on the metal surface, and at the resonance point, strong absorption of incident light takes place [28, 29]. Surface plasmon effects are, however, affected by several factors, which include the frequency of incident radiation, film thickness, and the formation of atomic islands on the surface of the dielectric substrate [30]. Therefore, this paper presents a quantitative analysis of the effect of deposition angle on the spectral and optical constants

of obliquely deposited ZnS/Ag nanofilms.

2. Materials and Methods

Glass slides were fixed on a rotary holder placed 11 cm away from the refractory boat inside the diffusion vacuum coater (Edwards AUTO 306). The substrate holder and the glass slide were set to an angle θ about the horizontal so that the vapour was incident obliquely to the substrate normal [31]. Silver metal wire (99.99% purity) was heated on a refractory tantalum boat under vacuum at a pressure of 2.5×10^{-5} m Bars and deposited on glass slide substrates. Three sets of samples of silver films of thickness 10 nm were deposited at different angles, $\theta = 0^o$, 30^o and 60^o.

The deposition of ZnS (99.99% purity) was done by heating ZnS crystals in a molybdenum boat with a source cover to reduce the spreading of the ZnS vapour. The ZnS was heated and deposited to a film thickness of 10 nm at an angle of incidence $\theta = 0$, 30, and 60^o on the glass slides previously coated with silver film to form the ZnS/Ag/glass multilayer system. The thickness monitor was calibrated separately for each of the materials in the vacuum chamber. The thickness of the films was measured by a thickness monitor connected to a quartz crystal monitoring system placed inside the diffusion chamber [32].

The spectral reflectance and transmittance of the samples were studied by the UV/Vis/NIR spectrometer (Perkin Elmer Lambda 19) with UV-WinLab software [33]. This is a double-beam instrument covering the ultraviolet, visible, and near-infrared spectral wavelengths. A baseline measurement using a clean piece of substrate was done. Reflectance was measured at an angle of incidence of 15^o to the optical system, while transmittance was measured at a normal angle of incidence to the multilayer in the wavelength range of 250 to 2500 nm [15, 34]. The refractive index n was calculated from the measured reflectance data given by equation (3). The energy band gap was determined by Tauc's method [22], [35] according to equation (7).

3. Results and Discussion

3.1 Spectral Measurements

In the proceeding sections, the figures in parenthesis before the ZnS/Ag nanofilms indicate film thickness, while the figures in parenthesis after ZnS and Ag represent the deposition angle of the respective nanomaterial.

3.1.1 Transmittance

The effect of deposition angle on the optical transmittance of ZnS/Ag nanostructures for normally deposited ZnS with Ag nanofilms deposited at different angles is presented in this section as shown in Figure 1. The transmittance measured for ZnS(0)/Ag(0), ZnS(0)/Ag(30) ZnS(0)/Ag(60) nanostructures Figure 1(a), had peaks of 54.9%, 61.3%, and 53.9% respectively, in the visible spectrum. The transmittance values showed that the oblique deposition of Ag increased optical transmission in the visible region [36]. The transmittance then decreased from the visible region towards the infrared spectral wavelengths.

When the deposition angle of ZnS was increased from 0^o to 30^o Figure 1(b), the transmittance in the visible region was slightly decreased. The transmittance values in the visible region had peaks at 55.8%, 48.6%, and 58.4% for ZnS(30)/Ag(0), ZnS(30)/Ag(30), and ZnS(30)/Ag(60), respectively. Whereas in the infrared region, the transmittance increased with the deposition angle of Ag, there was a general increase in transmittance in the infrared region due to the 30° oblique deposition angle of ZnS.

The transmittance values in the infrared region were slightly higher and more dispersed than those obtained in the infrared region of Figure 1(a). Therefore, ZnS reduced transmittance in the visible region but enhanced the transmittance of highly energetic electromagnetic radiation in the infrared wavelength [37].

When the deposition angle of ZnS was further raised to 60^o Figure 1(c), the transmittance in the visible region was further reduced compared to ZnS(30^o)/Ag nanostructures. The transmission peaks in the visible spectrum were 54.9%, 47.3%, and 50.1% for ZnS(60)/Ag(0), ZnS (60)/Ag(60), and ZnS (60)/Ag(60), respectively. The high transmittance of ZnS/Ag nano-multilayers in the visible wavelength was due to the high refractive index of ZnS which enhanced the antireflection of incident electromagnetic radiation [36, 38]. In the infrared region, at about λ = 800 nm, the transmittance was < 20% but further decreased rapidly with an increase in wavelength.

Thus, increasing the deposition angle of ZnS decreased transmittance in the visible region but increased transmittance in the infrared region due to the high deposition angle of ZnS. The physical significance of this observation was that oblique angle deposition had a negative contribution to transmittance in the visible region and a positive contribution in the infrared region. For purposes of solar thermal control and visibility in building envelopes, oblique depositions of ZnS should be done at near normal or very small angles to the substrate normal [34, 39].

3.1.2 Reflectance

The spectrophotometric measurements on reflectance were analysed on specimens fabricated at different deposition angles. The

reflectance of normally deposited ZnS(0)/Ag(0) nanofilms Figure 2(a), ranged between 5% and 35% in the visible range of the electromagnetic spectrum (400-800 nm), followed by a rise in reflectance to 41.1% in the infrared region at about λ = 810 nm. Remarkable interference effects were observed in the infrared region in all the samples. These effects were observed in the infrared region in the range of 800-2200 nm [40]. The interference effects disappeared or diminished as the wavelength approached the upper edge of the visible spectrum [6, 41].

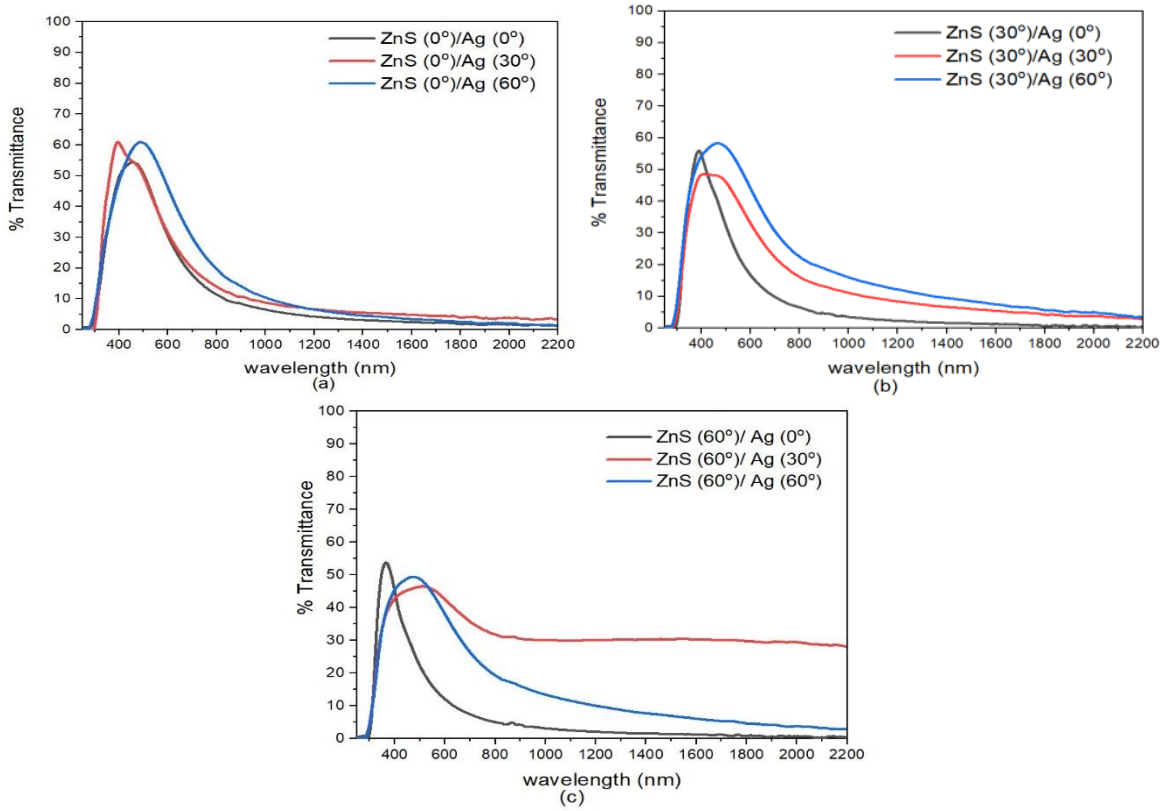

Figure 1. Variation of deposition angle with transmittance of ZnS/Ag nanofilms: (a) ZnS(0°) coated with Ag at different deposition angles; (b) ZnS(30°) coated with Ag at different deposition angles; (c) ZnS(60°) coated with Ag at different deposition angles.

When the thin films were deposited at ZnS(0)/Ag(30) Figure 2(b), the reflectance of (10 nm)ZnS(0)/Ag(30) in the visible region (400-800 nm of wavelength) was between 13% and 31%. The reflectance in the infrared region had a maximum value of 50.5%. The low value of reflectance was due to increased optical absorption in the ZnS/Ag nanostructures. Additionally, the increase in deposition angle increased film discontinuities and roughness, which in turn increased optical absorption due to the aggregation of silver islands in the nanostructures [42, 43]. Destructive interference enhanced optical absorption and transmittance but suppressed the reflectance of the electromagnetic waves [44]. There were interference effects that alternated with the deposition angle of silver nanofilms. This had pronounced effects on the reflectance of near-infrared radiation.

With the further increase in deposition angle of ZnS/Ag from ZnS(0)/Ag (30) to ZnS(0)/Ag (60) in Figure 2(c), the reflectance values further decreased. However, the multilayer angular response to reflectance was not so sensitive to the small increase in the deposition angle of silver metal films. The reduction in reflectance was attributed to atomic shadowing effects that created areas with reduced grain sizes of silver atoms [44]. This resulted in imperfections in the Ag nanofilms, which generated grain boundaries but in turn increased transmittance and decreased reflectance of the thin films. As the number of grain boundaries increased with an increase in deposition angle, there was a reduction in specular reflection for very thin films due to the scattering of incident light. The increase in reflectance at wavelengths λ > 800 nm was related to the increase in Drude-like absorption, in which the amount of voids in the metal phase increases [3, 44].

The interference effects in the infrared region in Figures 2(a), 2(b), and 2(c) were more intense in the ZnS(60)/Ag(60) nanofilms. These effects were a result of reflection from different optical interfaces of air-ZnS, ZnS-Ag, and Ag-glass interfaces [45-47]. There was a further rise in reflectance to about 54% in the infrared region at a wavelength of about 1300 nm. For wavelengths below 400 nm, there were interference minima in the reflectance of the samples. These effects were a result of an increase in

absorption due to inter-band electronic transitions of the zinc and silver atoms [41, 48].

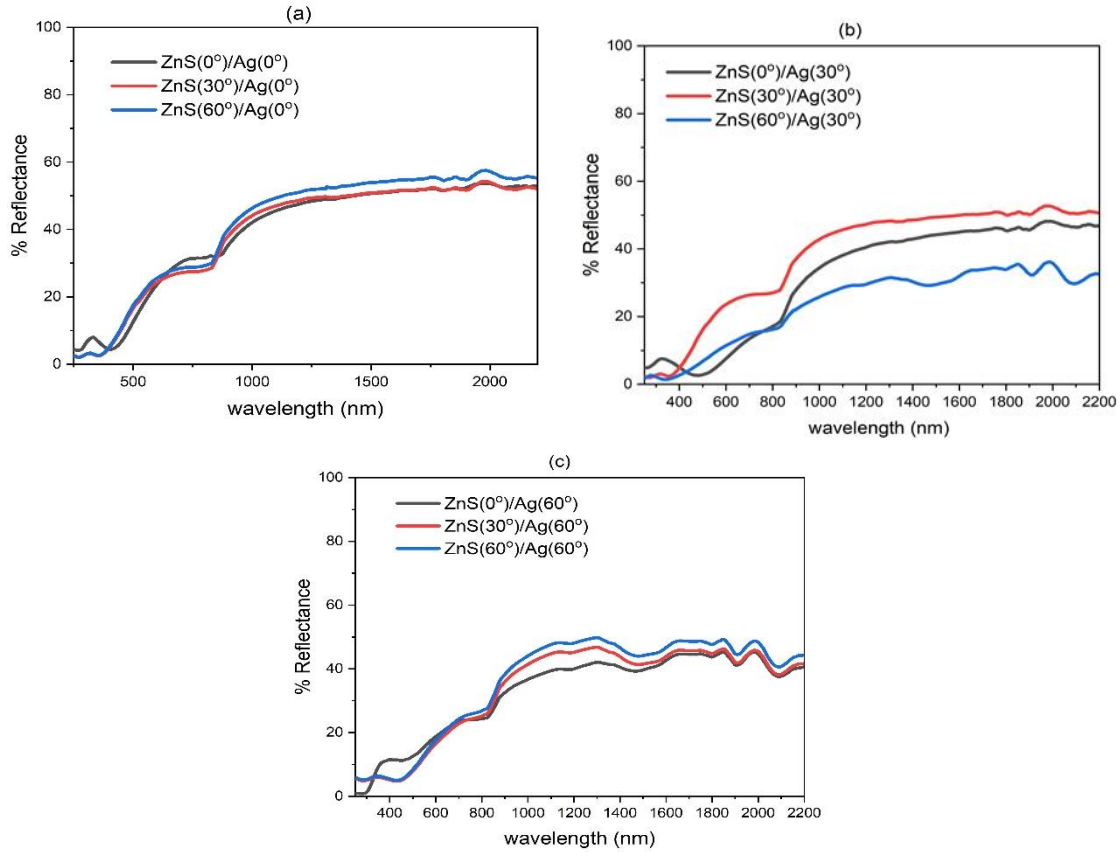

Figure 2. Reflectance spectra of ZnS/Ag nanostructures (a) The deposition angle of ZnS was increased from 0º to 60º when the deposition angle was fixed at 0º. (b) The deposition angle of ZnS was increased from 0º to 60º when the deposition angle was fixed at 30º. (c) The deposition angle of ZnS was increased from 0º to 60º when the deposition angle was fixed at 60º.

3.2 Optical Constants

The refractive index of the nanostructured ZnS/Ag nanofilms was calculated from the measured reflectance data according to equation (3) [18, 49]. The extinction coefficient (equation 4) of the material was determined from the absorption coefficient, $\alpha = 2.3026\frac{A}{d}$ which was calculated from the absorbance A of the electromagnetic waves during propagation through the material [16].

3.2.1 Effect of Deposition angle on refractive index and extinction coefficient

The effective refractive index of the (10 nm) ZnS/Ag nanofilms was observed to increase with an increase in wavelength but tends to remain constant in the wavelength range of 700-800 nm, as seen in Figures 3, 4, and 5. The values of refractive indices were lower in the visible region than in the infrared region. The low values of refractive index in the visible region were due to strong light absorption and the effect of quantum confinement [15, 50]. Beyond λ = 800 nm, the effective refractive index increased considerably, with maximum peaks observed in the near-infrared spectral regions.

When Ag was deposited at 0º to the substrate normal for different deposition angles of ZnS i.e., ZnS/Ag(0º), the refractive indices measured at wavelength λ = 1000 nm were n = 2.3, 5.0, and 5.4 for 0º, 30º, and 60º, respectively. These values of refractive index were very high for infrared radiation to pass through the nanofilms. Further increase in deposition angle of Ag to 30º, i.e., ZnS/Ag(30º) for the ZnS(30º)/Ag(0º) nanostructures, the refractive index measured at a wavelength of λ = 1000 nm for different deposition angles of ZnS were n = 3.7, 4.8, and 6.9 for 0º, 30º, and 60º, respectively. These values of refractive index are very high for infrared radiation to pass through the nanofilms [51, 52].

When the deposition angle of Ag was raised to 60º, i.e., ZnS/Ag(60º) nanofilms, the refractive index values measured at

wavelength λ = 1000 nm for different deposition angles of ZnS were n = 4.1, 4.7, and 5.0 for ZnS(0º)/Ag(0º), ZnS(30º)/Ag(0º) and ZnS(60º)/Ag(0º) respectively. However, the effective refractive index of the 10nm ZnS/Ag increased with an increase in the deposition angle of ZnS, both in the visible and infrared regions [39, 53]. The effective extinction coefficient was evaluated by equations (4) and (5). The effective extinction coefficient was observed to decrease from wavelength λ = 250 nm to small values at about λ = 380 nm. This observation was also reported by Jones [32] during the spectroscopic ellipsometry measurements of the refractive index of thin metal films. Beyond the wavelength of λ = 400 nm, there was an exponential increase in the effective extinction coefficient, with the Urbach tail hinged at 400 nm. This was due to the strong absorption of thermal radiation both in the visible and infrared spectral regions [52, 54].

When the deposition angle of silver was increased from 0º to 30º, there was a general decrease in the values of the effective refractive index and an increase in the values of the effective extinction coefficient Figure 4(b). This trend was observed in the visible and infrared spectral ranges. The decrease in the effective extinction coefficient in the infrared region was due to an increase in optical transmittance and low reflectance [55].

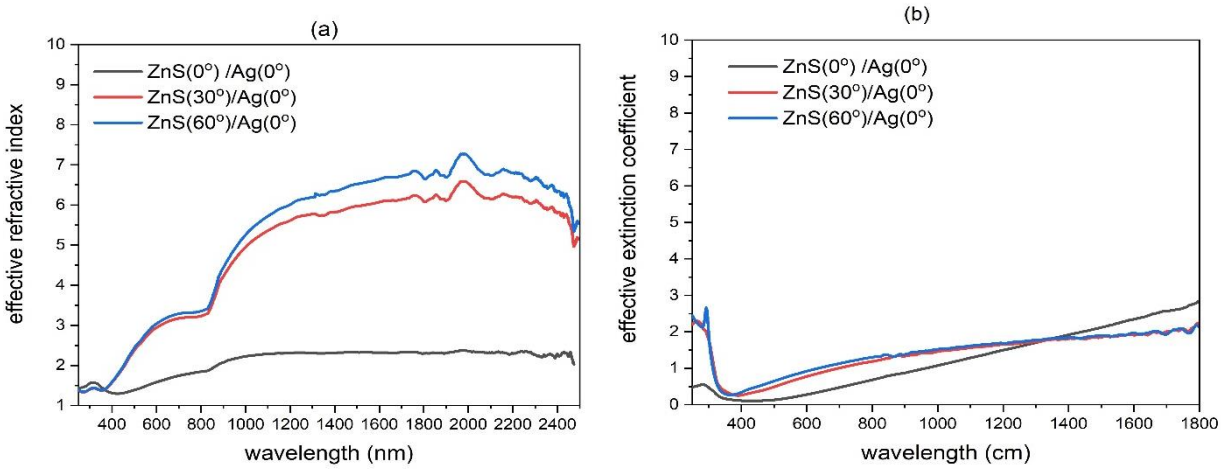

Figure 3. (a) Effect of deposition angle of ZnS on the effective refractive index with Ag nanofilms deposited at 0º; (b) Effect of deposition angle of ZnS on the effective extinction coefficient of ZnS/Ag nanofilms when Ag was deposited at different deposition angles.

A further increase in the deposition angle of silver decreased the effective refractive index (Figure 5(a)) but increased the effective extinction coefficient at the absorption edge Figure 5(b). This was due to a progressive increase in transmittance in the infrared region. The low effective extinction coefficient values in the visible region revealed low absorption loss. However, high values of the effective extinction coefficient in the infrared region imply a high loss of thermal energy contained in the infrared spectral region [53].

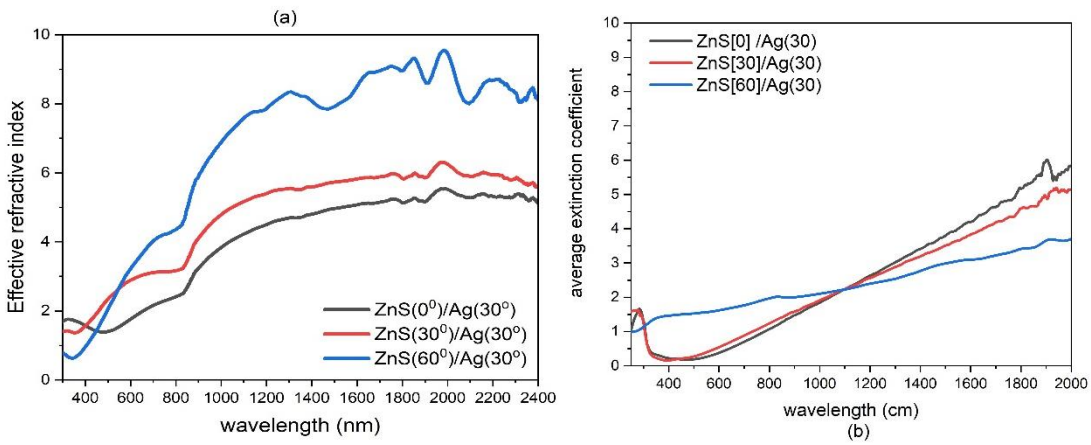

Figure 4. Effect of deposition angle of ZnS (a) refractive index of ZnS/Ag films at constant angle of deposition of Ag; (b) extinction coefficient of ZnS/Ag(30º) nanofilms at constant angle of deposition of Ag.

The low values of the effective refractive index in the visible wavelengths indicate that the nanofilms were transparent to visible light. The increase in the value of the effective refractive index in the infrared region and the decrease in the effective extinction coefficient at the absorption edge could be explained by high light absorption or scattering [56]. The increase in the effective extinction coefficient with deposition angle indicates that the light traveling through ZnS/Ag nanofilms experienced attenuation due to loss of energy. This may be accounted for by various loss mechanisms such as generation of phonons, scattering, crystallite size, and a less dense layer structure whose density decreased with an increase in deposition [43], [57], [58].

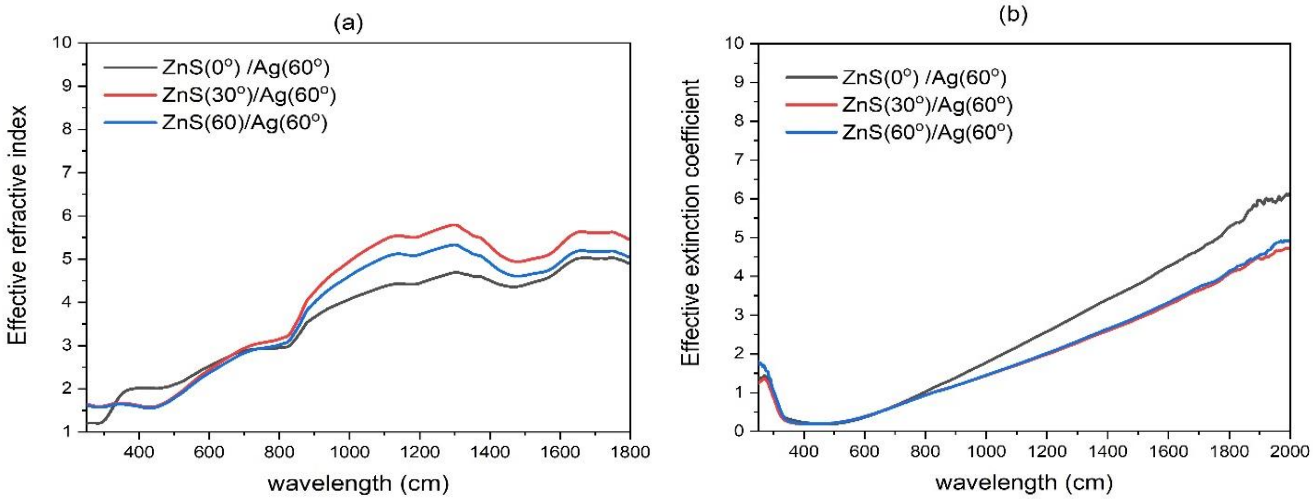

Figure 5. Effect of deposition angle of ZnS on (a) refractive index of ZnS/Ag films at constant angle of deposition of Ag. (b) extinction coefficient of ZnS/Ag(60º) nanofilms at constant angle of deposition of Ag.

3.3 The energy band gap

The energy gap of the nanofilms was determined from the absorption coefficient (α), equation (5), which was calculated from the transmittance (T) of the ZnS/Ag thin films [59].

3.3.1 Effect of deposition angle on the band gap energy of ZnS/Ag nanofilms

Using equation 7, a plot of $(\alpha h\nu)^2$ against photon energy $h\nu$ is shown in Figure 6. From the graph, the linear potions were tilted toward the right along the $h\nu$ axis with a very steep slope. The increase in energy band gap in Figure 6(a), (b), and (c) was due to an increase in confinement effects brought about by an increase in deposition angle [60]. The energy band gaps for ZnS(0º)/Ag(0º), ZnS(30º)/Ag(0º), and ZnS(60º)/Ag(0º) Figure 6(a) were 3.62 eV, 3.68 eV, and 3.77 eV, respectively. In a separate study by Bartek *et al.*, [22], it was observed that the absorption edge occurred in the range of 2.23 eV to 3.45 eV due to defects in the band gap energy.

When the deposition angle of silver was increased to 30º Figure 6(b), the energy band gaps for ZnS(0º)/Ag(30º), ZnS(30º)/Ag(30º), and ZnS(60º)/Ag(30º) were 3.79 eV, 3.87 eV, and 3.83 eV, respectively. A further increase in the deposition angle of silver to 60º (Figure 6(c)) increased the energy band gap of the nanofilms.

The energy band gaps for ZnS(0º)/Ag(60º), ZnS(30º)/Ag(60º), and ZnS(60º)/Ag(60º) were 3.95 eV, 3.99 eV, and 3.87 eV, respectively. The small film thickness and increase in deposition angle gave high values for the optical band gap. All the ZnS/Ag nanofilms exhibited minima values in the range of 2.49 eV to 3.25 eV. The high band gap was due to nanocrystallite sizes and crystal imperfections. Nevertheless, the high band gap energy can be explained in terms of quantum confinement effects that were associated with the existence of nanocrystallites and the small film thickness [61]. This allowed the transmission of visible wavelengths but prevented the transmission of low-energy infrared radiation [20, 62, 63].

The energy band gaps for ZnS(0º)/Ag(60º), ZnS(30º)/Ag(60º), and ZnS(60º)/Ag(60º) were 3.95 eV, 3.99 eV, and 3.87 eV, respectively. The small film thickness and increase in deposition angle gave high values for the optical band gap. All the ZnS/Ag nanofilms exhibited minima values in the range of 2.49 eV to 3.25 eV. The high band gap was due to nanocrystallite sizes and crystal imperfections. Nevertheless, the high band gap energy can be explained in terms of quantum confinement effects that are associated with the existence of nanocrystallites and the small film thickness. This allowed the transmission of light energy from the visible band but prevented the transmission of low-energy infrared radiation [20, 37, 62].

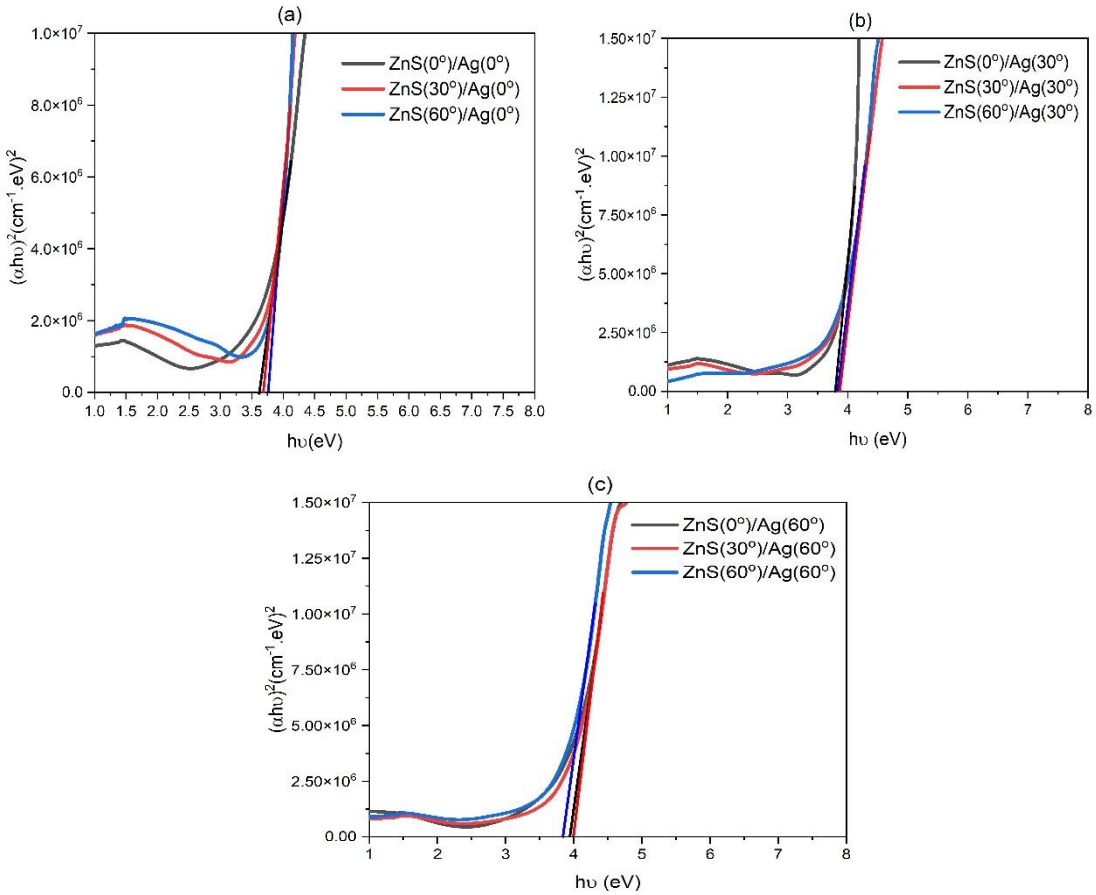

Figure 6. Effect of deposition angle on energy band gap: (a) deposition angle of ZnS was increased as the deposition angle of Ag was kept at 0°; (b) the deposition angle of ZnS was increased as the deposition angle of Ag was maintained at 30°; (c) the deposition angle of ZnS was increased as the deposition Ag was maintained at 60°.

However, the increase in the deposition angle of ZnS from 0° to 60° had minimal impact on the variation of the energy band gap with the deposition angle. On the other hand, the increase in the deposition angle of silver increased the energy band. This trend was observed in Figures 6(a), (b), and (c) after extra plotting along the Urbach region of each plot.

4. Conclusions

The optical transmittance of ZnS/Ag nanofilms in the visible region was enhanced by the deposition of silver nanoparticles at higher deposition angles. However, the deposition of Ag nanoparticles at high deposition angles suppressed the optical transmittance in the infrared region. The reflectance of evaporated ZnS/Ag nanofilms decreased with a decrease in the deposition angle of ZnS. However, the reflectance decreased with an increase in the deposition angle of silver metal films. An increase in the deposition angle of silver decreased the effective refractive index. The effective refractive index increased from 3.25 in the visible spectrum to 6.2 in the infrared spectrum. The low values of the effective refractive index in the visible wavelengths indicate that the nanofilms were transparent to visible light. The extinction coefficient increased from an average of 0.2 at about 400nm toward the infrared spectral range. The increase in deposition of ZnS did not significantly affect the energy band gap. However, the increase in the deposition angle of silver increased the energy band of the nanofilms from 3.52 to 3.99 eV.

Acknowledgments

The authors would like to acknowledge the financial and material support from the Uganda Independent Scholarships Trust Fund Board, the Ministry of Education and Sports and the Swedish International Cooperation Agency (SIDA) through the International Science Programme (ISP), Uppsala University.

References

[1] Bwayo, E., & Obwoya, S. K. (2014). Coefficient of Thermal Diffusivity of Insulation Brick Developed from Sawdust and Clays. Journal of Ceramics, 2014, 1-6. https://doi.org/10.1155/2014/861726.

[2] Fang, B., YangC., Shen, W., Zhang, X., Zhang, Y., & Liu, X. (2017). Highly efficient omnidirectional structural color tuning method based on dielectric–metal–dielectric structure. Applied Optics, 56(4), 175-180.

[3] Multilayer, M. C., Nur-e-alam, M., Rahman, M., & Basher, M. K. (2020). Thin-Film Structures Prepared by RF.

[4] Chambouleyron, I., & Martinez, J. M. (2002). Optical properties of dielectric and semiconductor thin films. Handbook of Thin Films, 3, 593-622. https://doi.org/10.1016/b978-012512908-4/50048-5.

[5] Davalos, J. A. G., Carvano, J. M., & Blanco, J. (2017). Numerical determination of visible/NIR optical constants from laboratory spectra of HED meteorites. Icarus, 285, 275-290. https://doi.org/10.1016/j.icarus.2016.10.022.

[6] Sakkas, C., Rauch, J. Y., Cote, J. M., Tissot, V., Gavoille, J., & Martin, N. (2021). Tuning the optical properties of WO3 films exhibiting a zigzag columnar microstructure. Coatings, 11(4). https://doi.org/10.3390/coatings11040438.

[7] Włodarski, M., Chodorow, U., Jóźwiak, S., Putkonen, M., Durejko, T., Sajavaara, T., & Norek, M. (2019). Structural and optical characterization of ZnS ultrathin films prepared by low-temperature ALD from diethylzinc and 1.5-pentanedithiol after various annealing treatments. Materials, 12(19), 1-16. https://doi.org/10.3390/ma12193212.

[8] Peng, S., Yang, X., Yang, Y., Wang, S., Zhou, Y., Hu, J., Li, Q., & He, J. (2019). Direct Detection of Local Electric Polarization in the Interfacial Region in Ferroelectric Polymer Nanocomposites. Advanced Materials, 31(21), 1-9. https://doi.org/10.1002/adma.201807722.

[9] Sun, X., Hu, K., Tu, J., & Chen, K. (2021). Design and preparation of superhydrophobic, broadband and double-layer antireflective coatings. Surfaces and Interfaces, 24(March). https://doi.org/10.1016/j.surfin.2021.101135.

[10] Sharma, N., Sharma, S., Prabakar, K., Amirthapandian, S., Ilango, S., Dash, S., & Tyagi, A. K. (2015). C. Substrate temperature induced microstructural transition from amorphous at RT, nanocrystalline at 300. ArXiv.

[11] Charles, C., Martin, N., & Devel, M. (2015). Optical properties of nanostructured WO3 thin films by GLancing Angle Deposition: Comparison between experiment and simulation. Surface and Coatings Technology, 276, 136-140. https://doi.org/10.1016/J.SURFCOAT.2015.06.051.

[12] Dalapati, G. K., Kushwaha, A. K., Sharma, M., Suresh, V., Shannigrahi, S., Zhuk, S., & Masudy-Panah, S. (2018). Transparent heat regulating (THR) materials and coatings for energy saving window applications: Impact of materials design, micro-structural, and interface quality on the THR performance. Progress in Materials Science, 95, 42-131.

[13] Taylor, R. A., Hewakuruppu, Y., DeJarnette, D., & Otanicar, T. P. (2016). Comparison of selective transmitters for solar thermal applications. Applied Optics, 55(14), 3829. https://doi.org/10.1364/ao.55.003829.

[14] Baetens, R., Jelle, B. P., & Gustavsen, A. (2010). Properties, requirements and possibilities of smart windows for dynamic daylight and solar energy control in buildings: A state-of-the-art review. Solar Energy Materials and Solar Cells, 94(2), 87-105.

[15] Ding, G., & Clavero, C. (2017). Silver-Based Low-Emissivity Coating Technology for Energy-Saving Window Applications. Modern Technologies for Creating the Thin-Film Systems and Coatings. https://doi.org/10.5772/67085.

[16] Sharma, M., Sen, S., Gupta, J., Ghosh, M., Pitale, S., Gupta, V., & Gadkari, S. C. (2018). Tunable blue-green emission from ZnS(Ag) nanostructures grown by hydrothermal synthesis. Journal of Materials Research, 33(23), 3963-3970. https://doi.org/10.1557/jmr.2018.358.

[17] Sönmezolu, S., Arslan, A., Serin, T., & Serin, N. (2011). The effects of film thickness on the optical properties of TiO 2-SnO2 compound thin films. Physica Scripta, 84(6). https://doi.org/10.1088/0031-8949/84/06/065602.

[18] Ramzan, M., Rana, A. M., Ahmed, E., Bhatti, A. S., Hafeez, M., Ali, A., & Nadeem, M. Y. (2014). Optical description of HfO2/Al/HfO2 multilayer thin film devices. Current Applied Physics, 14(12), 1854-1860. https://doi.org/10.1016/j.cap.2014.10.023.

[19] Haus, J. W., Katte, N., Serushema, J.-B., & Scalora, M. (2010). Metallodielectrics as metamaterials. Active Photonic Materials III, 7756(September 2010), 77560F. https://doi.org/10.1117/12.862407.

[20] Huang, L., Wang, T., Li, X., Wang, X., Zhang, W., Yang, Y., & Tang, Y. (2020). UV-to-IR highly transparent ultrathin diamond nanofilms with intriguing performances: Anti-fogging, self-cleaning and self-lubricating. Applied Surface Science, 527, 146733. https://doi.org/10.1016/j.apsusc.2020.146733.

[21] Khan, S. B., Wu, H., Ma, L., Hou, M., & Zhang, Z. (2017). HfO2 Nanorod Array as High-Performance and High-Temperature Antireflective Coating. Advanced Materials Interfaces, 4(6), 1-9. https://doi.org/10.1002/admi.201600892.

[22] Bartek, N., Shvartsman, V. V., Lupascu, D. C., Prah, U., & Uršič, H. (2019). Influence of synthesis route on the properties of lead iron niobate. 2019 IEEE International Symposium on Applications of Ferroelectrics, ISAF 2019 - Proceedings, 1-4.

https://doi.org/10.1109/ISAF43169.2019.9034943.

[23] Bashir, K., Ali, A., Ashraf, M., Mehboob, N., & Zaman, A. (2021). Optical and structural properties of vacuum annealed multilayer nanostructured CdZnS thin films deposited by thermal evaporation. Optical Materials, 119(May), 111353. https://doi.org/10.1016/j.optmat.2021.111353.

[24] Savaloni, H., & Savari, R. (2018). Nano-structural variations of ZnO:N thin films as a function of deposition angle and annealing conditions: XRD, AFM, FESEM and EDS analyses. In Materials Chemistry and Physics (Vol. 214). https://doi.org/10.1016/j.matchemphys.2018.04.099.

[25] Boubaia, A., Assali, A., Berrah, S., Bennacer, H., Zerifi, I., & Boukortt, A. (2021). Band gap and emission wavelength tuning of Sr-doped BaTiO3 (BST) perovskites for high-efficiency visible-light emitters and solar cells. Materials Science in Semiconductor Processing, 130(November 2020), 105837. https://doi.org/10.1016/j.mssp.2021.105837.

[26] Rhodes, C., Cerruti, M., Efremenko, A., Losego, M., Aspnes, D. E., Maria, J. P., & Franzen, S. (2008). Dependence of plasmon polaritons on the thickness of indium tin oxide thin films. Journal of Applied Physics, 103(9). https://doi.org/10.1063/1.2908862.

[27] Chalana, S. R., Ganesan, V., & Mahadevan Pillai, V. P. (2015). Surface plasmon resonance in nanostructured Ag incorporated ZnS films. AIP Advances, 5(10), 107207.

[28] Blake, J. C., Rossi, S., Jonsson, M. P., & Dahlin, A. (2022). Scalable Reflective Plasmonic Structural Colors from Nanoparticles and Cavity Resonances – the Cyan-Magenta-Yellow Approach. Advanced Optical Materials, 10(13). https://doi.org/10.1002/adom.202200471.

[29] Vrakatseli, V. E., Kalarakis, A. N., Kalampounias, A. G., Amanatides, E. K., & Mataras, D. S. (2018). Glancing angle deposition effect on structure and light-induced wettability of RF-sputtered TiO2 thin films. Micromachines, 9(8). https://doi.org/10.3390/mi9080389.

[30] Diab, M., & Alabbosh, O. (2018). Studying of Thickness Effects on the Optical and Structural Properties of ZnO / Ag / ZnO Multilayer Thin Films by Using Surface Plasmon Resonance. 70, 27-30.

[31] Chaffar Akkari, F., Ben Jbara, H., Abdelkader, D., Gallas, B., & Kanzari, M. (2018). Effect of angle deposition γ on the structural, optical and electrical properties of copper oxide zigzag (+γ, −γ) nanostructures elaborated by glancing angle deposition. Thin Solid Films, 657, 61-69. https://doi.org/10.1016/j.tsf.2018.05.006.

[32] Jones, A., Uggalla, L., Li, K., Fan, Y., Willow, A., Mills, C. A., & Copner, N. (2021). Continuous in-line chromium coating thickness measurement methodologies: An investigation of current and potential technology. Sensors, 21(10). https://doi.org/10.3390/s21103340.

[33] Studenikin, S. A., Golego, N., & Cocivera, M. (1998). Optical and electrical properties of undoped ZnO films grown by spray pyrolysis of zinc nitrate solution. Journal of Applied Physics, 83(4), 2104-2111. https://doi.org/10.1063/1.366944.

[34] Garlisi, C., Trepci, E., Li, X., Al Sakkaf, R., Al-Ali, K., Nogueira, R. P., Zheng, L., Azar, E., & Palmisano, G. (2020). Multilayer thin film structures for multifunctional glass: Self-cleaning, antireflective and energy-saving properties. Applied Energy, 264(February). https://doi.org/10.1016/j.apenergy.2020.114697.

[35] Bashir, K., Ali, A., Ashraf, M., Mehboob, N., & Zaman, A. (2021). Optical and structural properties of vacuum annealed multilayer nanostructured CdZnS thin films deposited by thermal evaporation. Optical Materials, 119(May). https://doi.org/10.1016/j.optmat.2021.111353.

[36] He, C. Y., Gao, X. H., Yu, D. M., Guo, H. X., Zhao, S. S., & Liu, G. (2021). Highly Enhanced Thermal Robustness and Photothermal Conversion Efficiency of Solar-Selective Absorbers Enabled by High-Entropy Alloy Nitride MoTaTiCrN Nanofilms. ACS Applied Materials and Interfaces, 13(14), 16987-16996. https://doi.org/10.1021/acsami.0c23011.

[37] Zhao, Y., Xu, R., Zhang, X., Hu, X., Knize, R. J., & Lu, Y. (2013). Simulation of smart windows in the ZnO/VO2/ZnS sandwiched structure with improved thermochromic properties. Energy and Buildings, 66, 545-552. https://doi.org/10.1016/j.enbuild.2013.07.071.

[38] Cho, H., Yun, C., Park, J.-W., & Yoo, S. (2009). Highly flexible organic light-emitting diodes based on ZnS/Ag/WO3 multilayer transparent electrodes. Organic Electronics, 10(6), 1163-1169.

[39] Osanyinlusi, O., Mukolu, A. I., & Zebaze Kana, M. G. (2016). Structural and optical properties of Al/ZnO thin films deposited by radio frequency sputtering. Materials Research Express, 3(9), 1-9. https://doi.org/10.1088/2053-1591/3/9/096401.

[40] Lou, R., Zhang, G., Li, G., Li, X., Liu, Q., & Cheng, G. (2020). Design and fabrication of dual-scale broadband antireflective structures on metal surfaces by using nanosecond and femtosecond lasers. Micromachines, 11(1). https://doi.org/10.3390/mi11010020.

[41] Włodarski, M., Chodorow, U., Jóźwiak, S., Putkonen, M., Durejko, T., Sajavaara, T., & Norek, M. (2019). Structural and Optical Characterization of ZnS Ultrathin Films Prepared by Low-Temperature ALD from Diethylzinc and 1.5-Pentanedithiol after Various Annealing Treatments. Materials, 12(19), 3212.

[42] Cho, K. H., Ahn, S. Il, Lee, S. M., Choi, C. S., & Choi, K. C. (2010). Surface plasmonic controllable enhanced emission from the intrachain and interchain excitons of a conjugated polymer. Applied Physics Letters, 97(19). https://doi.org/10.1063/1.3508949.

[43] Lee, G.-J., & Wu, J. J. (2017). Recent developments in ZnS photocatalysts from synthesis to photocatalytic applications—A review. Powder Technology, 318, 8-22.

[44] He, Y., Basnet, P., Murph, S. E. H., & Zhao, Y. (2013). Ag nanoparticle embedded TiO2 composite nanorod arrays fabricated by oblique angle deposition: Toward plasmonic photocatalysis. ACS Applied Materials and Interfaces, 5(22), 11818-11827. https://doi.org/10.1021/am4035015.

[45] Al Garni, S. E., & Qasrawi, A. F. (2017). Effect of Indium nano-sandwiching on the structural and optical performance of ZnSe films. Results in Physics, 7, 4168-4173. https://doi.org/10.1016/j.rinp.2017.10.040.

[46] Multilayer, M. C., Nur-e-alam, M., Rahman, M., & Basher, M. K. (2020). Thin-Film Structures Prepared by RF.

[47] Vrakatseli, V. E., Kalarakis, A. N., Kalampounias, A. G., Amanatides, E. K., & Mataras, D. S. (2018). Glancing angle deposition effect on structure and light-induced wettability of RF-sputtered TiO2 thin films. Micromachines, 9(8), 389.

[48] Zhou, C., & Liu, H. (2017). A novel nanofibrous film chemosensor for highly selective and sensitive optical signaling of Zn2+. Journal of the Brazilian Chemical Society, 28(10), 1947-1952. https://doi.org/10.21577/0103-5053.20170036.

[49] Sönmezoğlu, S., Termeli, T. A., Akin, S., & Askeroğlu, I. (2013). Synthesis and characterization of tellurium-doped CdO nanoparticles thin films by sol-gel method. Journal of Sol-Gel Science and Technology, 67(1), 97-104. https://doi.org/10.1007/s10971-013-3054-1.

[50] Pan, Y., Fan, Y., & Niu, J. (2020). Optical properties of ultra-thin silver films deposited by thermal evaporation and its application in optical filters. Infrared Physics and Technology, 104, 103123. https://doi.org/10.1016/j.infrared.2019.103123.

[51] Granqvist, C. G., Arvizu, M. A., Bayrak Pehlivan, Qu, H. Y., Wen, R. T., & Niklasson, G. A. (2018). Electrochromic materials and devices for energy efficiency and human comfort in buildings: A critical review. Electrochimica Acta, 259, 1170-1182. https://doi.org/10.1016/j.electacta.2017.11.169.

[52] Veziroglu, S., Ullrich, M., Hussain, M., Drewes, J., Shondo, J., Strunskus, T., Adam, J., Faupel, F., & Aktas, O. C. (2020). Plasmonic and non-plasmonic contributions on photocatalytic activity of Au-TiO2 thin film under mixed UV–visible light. Surface and Coatings Technology, 389, 125613. https://doi.org/10.1016/j.surfcoat.2020.125613.

[53] Hadia, N. M. A., Mohamed, W. S., & Abd El-sadek, M. S. (2019). Simultaneous synthesis of various Sb2S3 nanostructures by vapor transport technique. Materials Chemistry and Physics, 235(March), 121750. https://doi.org/10.1016/j.matchemphys.2019.121750.

[54] Patil, R. G., Yerudkar, A. N., Joglekar, A. R., Panse, S. V., Dalvi, V. H., Shankarling, G. S., Deshpande, V. D., Nayak, A. K., & Joshi, J. B. (2022). Transition metal compounds as solar selective material. Reviews in Chemical Engineering, 38(6), 669-702. https://doi.org/10.1515/revce-2020-0026.

[55] Hassanien, A. S., & Akl, A. A. (2016). Effect of Se addition on optical and electrical properties of chalcogenide CdSSe thin films. Superlattices and Microstructures, 89, 153-169. https://doi.org/10.1016/j.spmi.2015.10.044.

[56] Khalef, W. K., Mohammed, S. R., Salman, A. A., Shukur, N. J., Yousif, B. A., Al-Baghdadi, S. B., & Faisal, A. D. (2018). Oblique angle deposition of cadmium oxide film on quartz substrate. International Journal of Nanoelectronics and Materials, 11(Special Issue BOND21), 23-30.

[57] Han, Y., Dong, S., Shao, J., Fan, W., & Chi, C. (2021). Synthesis of a Sidewall Fragment of a (12,0) Carbon Nanotube. Angewandte Chemie, 133(5), 2690-2694. https://doi.org/10.1002/ange.202012651.

[58] Kumar, S., Kumar, S., Sharma, P., Sharma, V., & Katyal, S. C. (2012). CdS nanofilms: Effect of film thickness on morphology and optical band gap. Journal of Applied Physics, 112(12). https://doi.org/10.1063/1.4769799.

[59] Pedrosa, P., Ferreira, A., Cote, J.-M., Martin, N., Yazdi, M. A. P., Billard, A., Lanceros-Mendez, S., & Vaz, F. (2017). Influence of the sputtering pressure on the morphological features and electrical resistivity anisotropy of nanostructured titanium films. Applied Surface Science, 420, 681-690.

[60] Bilal, U., Ramzan, M., Imran, M., Naz, G., Mukhtar, M. W., Fahim, F., & Iqbal, H. M. N. (2022). HfO2-based nanostructured thin-films (i.e., low-e coatings) with robust optical performance and energy efficiency. Journal of Nanostructure in Chemistry, 12(6), 1131-1142. https://doi.org/10.1007/s40097-022-00485-2.

[61] Saha, A., Figueroba, A., & Konstantatos, G. (2020). Ag2ZnSnS4 Nanocrystals Expand the Availability of RoHS Compliant Colloidal Quantum Dots. Chemistry of Materials, 32(5), 2148-2155. https://doi.org/10.1021/acs.chemmater.9b05370.

[62] Sharma, S. S., Palaty, S., & John, A. K. (2021). Band gap modified zinc oxide nanoparticles: an efficient visible light active catalyst for wastewater treatment. International Journal of Environmental Science and Technology, 18(9), 2619-2632. https://doi.org/10.1007/s13762-020-02976-7.

[63] Zhang, X., Bao, N., Ramasamy, K., Wang, Y. H. A., Wang, Y., Lin, B., & Gupta, A. (2012). Crystal phase-controlled synthesis of Cu2FeSnS4 nanocrystals with a band gap of around 1.5 eV. Chemical Communications, 48(41), 4956-4958. https://doi.org/10.1039/c2cc31648j.